

See discussions, stats, and author profiles for this publication at: <https://www.researchgate.net/publication/235384082>

Intercalation Pathway in Many-Particle LiFePO₄ Electrode Revealed by Nanoscale State-of-Charge Mapping

ARTICLE in NANO LETTERS · JANUARY 2013

Impact Factor: 13.59 · DOI: 10.1021/nl3031899 · Source: PubMed

CITATIONS

68

READS

110

10 AUTHORS, INCLUDING:



[Josh Sugar](#)

Sandia National Laboratories

33 PUBLICATIONS 314 CITATIONS

[SEE PROFILE](#)



[Kevin Zavadil](#)

Sandia National Laboratories

101 PUBLICATIONS 723 CITATIONS

[SEE PROFILE](#)



[Tolek Tyliszczak](#)

Lawrence Berkeley National Laboratory

353 PUBLICATIONS 6,844 CITATIONS

[SEE PROFILE](#)



[Wei Lai](#)

Michigan State University

27 PUBLICATIONS 615 CITATIONS

[SEE PROFILE](#)

Intercalation Pathway in Many-Particle LiFePO₄ Electrode Revealed by Nanoscale State-of-Charge Mapping

William C. Chueh,^{*,†,⊥} Farid El Gabaly,[†] Joshua D. Sugar,[†] Norman C. Bartelt,[†] Anthony H. McDaniel,[†] Kyle R. Fenton,[‡] Kevin R. Zavadil,[‡] Tolek Tyliszczak,[§] Wei Lai,^{||} and Kevin F. McCarty[†]

[†]Sandia National Laboratories, Livermore, California 94551, United States

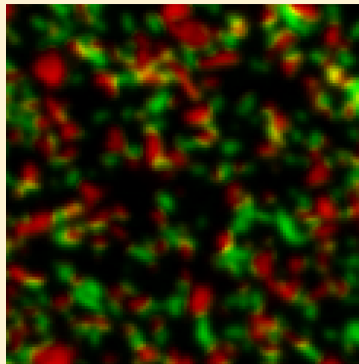
[‡]Sandia National Laboratories, Albuquerque, New Mexico, 87185, United States

[§]Advanced Light Source, Lawrence Berkeley National Laboratory, Berkeley, California 94720, United States

^{||}Department of Chemical Engineering and Materials Science, Michigan State University, East Lansing, Michigan 48824, United States

Supporting Information

ABSTRACT: The intercalation pathway of lithium iron phosphate (LFP) in the positive electrode of a lithium-ion battery was probed at the ~40 nm length scale using oxidation-state-sensitive X-ray microscopy. Combined with morphological observations of the same exact locations using transmission electron microscopy, we quantified the local state-of-charge of approximately 450 individual LFP particles over nearly the entire thickness of the porous electrode. With the electrode charged to 50% state-of-charge in 0.5 h, we observed that the overwhelming majority of particles were either almost completely delithiated or lithiated. Specifically, only ~2% of individual particles were at an intermediate state-of-charge. From this small fraction of particles that were actively undergoing delithiation, we conclude that the time needed to charge a particle is ~1/50 the time needed to charge the entire particle ensemble. Surprisingly, we observed a very weak correlation between the sequence of delithiation and the particle size, contrary to the common expectation that smaller particles delithiate before larger ones. Our quantitative results unambiguously confirm the mosaic (particle-by-particle) pathway of intercalation and suggest that the rate-limiting process of charging is initiating the phase transformation by, for example, a nucleation-like event. Therefore, strategies for further enhancing the performance of LFP electrodes should not focus on increasing the phase-boundary velocity but on the rate of phase-transformation initiation.



KEYWORDS: Lithium iron phosphate, STXM, X-ray absorption spectroscopy, phase transformation, mosaic

Among the most intensely investigated materials for the positive electrodes of lithium-ion batteries is Li_xFePO₄ (LFP, with $0 \leq x \leq 1$). LFP undergoes a first-order phase transformation at well-defined compositions when lithium is added or removed, leading to lithium-rich and lithium-poor phases.¹ Understanding the lithium intercalation pathway in LFP is of crucial technological importance, as the intercalation kinetics directly determines the current density and efficiency of the electrode. In the past few years, significant progress has been made in understanding the LFP phase transformation, especially of single LFP particles.^{2–9} A solid-solution pathway was also proposed based on first-principles¹⁰ and phase-field modeling.^{11,12} In this pathway, a particle cycles between FePO₄ and LiFePO₄ without having coexisting phases. That is, phase separation is suppressed in the nominally two-phase region.

One of the most controversial topics surrounding lithium intercalation in LFP is its behavior in a realistic battery electrode, that is, under constant current conditions in a many-particle ensemble with a broad distribution of particle sizes. Experimentally, lithium intercalation and phase transformation in LFP ensembles have been studied using a wide range of techniques including *in situ* X-ray and neutron diffraction^{13–18}

(typically averaging over the entire electrode), transmission electron microscopy^{19–22} (typically sampling only a few particles), and electrochemical methods.^{23,24} Microdiffraction²⁵ at a resolution of several micrometers has also been employed. Some results suggest that LFP transforms concurrently in almost all particles.^{16,19} Other results support a particle-by-particle intercalation pathway,²¹ originally proposed for LFP by Delmas et al.,¹³ whereby only a small fraction of the particles undergoes phase transformation at any given time. Two phases coexist within the particle ensemble but not within single particles, contrary to the “concurrent” intercalation pathway. The electrode forms a “mosaic” of homogeneous particles that are mostly either lithium-rich or lithium-poor.^{5,6,12,13,26–28} The origin of the mosaic pathway remains unclear and has been attributed to minimization of the interfacial energy,⁵ rapid phase boundary movement,¹³ and fast interparticle transport.^{6,28} In the experimental work so far, the lack of spatial resolution or statistical relevance likely accounts for some of the

Received: August 27, 2012

Revised: December 31, 2012

Published: January 30, 2013



discrepancies. The ability to image the local state-of-charge of a large number of particles that span the thickness of the electrode is needed to clarify the intercalation pathway in many-particle LFP electrodes.

In this work, we employed synchrotron-based scanning transmission X-ray microscopy (STXM) at the Advanced Light Source (beamline 5.3.2)²⁹ and transmission electron microscopy (TEM) to image the local state-of-charge and particle morphology, respectively, of a LFP electrode from a cycled coin-cell battery. We spanned the length scales of individual particles as well as the macroscopic electrode ensemble. The local state-of-charge within individual particle is determined from Fe L_3 near-edge X-ray absorption spectra taken at a lateral step size of 40 nm. We imaged approximately 450 individual LFP particles across the thickness of the electrode. We show unambiguously that delithiation under a moderately high charging rate of 1 C (where it takes 1 h to charge the electrode to full capacity) proceeds via the particle-by-particle pathway. In fact, the fraction of particles that are actively undergoing delithiation (at 50% state-of-charge) is remarkably small, only ~2%. A statistical analysis reveals a weak correlation between state-of-charge and particle size, indicating that there is little preference to delithiate small or large particles selectively.

Standard coin battery cells consisting of an ~35 μm thick carbon-coated LFP/graphite composite cathode, Li anode, and 1.2 M LiPF₆/ethylene carbonate/ethyl methyl carbonate electrolyte were electrochemically cycled five times. A stable capacity of 150 mAh g⁻¹ was obtained (see Supporting Information for details). Reference Fe L_3 absorption spectra from the limiting compositions LiFePO₄ and FePO₄ were obtained from battery cells at 0 and 100% state-of-charge prepared by discharging and charging at 1/50 C, respectively. We then charged a battery to 75 mAh g⁻¹ (50% state-of-charge) at 1 C. Immediately upon reaching the target state-of-charge, we rapidly disassembled the cell inside a dry room and washed the electrode with an excess of dimethyl carbonate. This procedure was completed within ~4 min after terminating the charge. Finally, the composite electrode was mechanically cross-sectioned to yield an ~400 nm thick sample. Because charging was terminated within the electrode's voltage plateau, we expect the difference in the chemical potential between lithium-rich and lithium-poor particles to be very small (mainly due to morphology differences),³⁰ providing only a weak driving force for the redistribution of lithium between particles. Furthermore, because the LFP particles are coated with carbon, solid-state lithium ion transport between particles after removing the electrolyte is unlikely. Therefore, we assume that no significant intraparticle transport occurs after removing the applied current. We recognize, however, that lithium can redistribute within each particle without external mass transport.^{10,12}

Each STXM spectral-image consisted of ~15 000 nanoscale X-ray absorption spectra obtained by rastering the X-ray beam and scanning its energy over the Fe L_3 edge. These spectral-images give local chemical information averaged in the direction of the beam, that is, through the sample thickness. The moderate thickness ensures that the X-rays are not totally absorbed. Absorption spectra from the reference samples showed negligible spatial variations. The reference spectra were obtained by averaging across several particles (Figure 1). Consistent with previous reports, a change in the Fe oxidation state (from 2+ to 3+) upon delithiation shifts the main absorption feature in the Fe L_3 edge from ~708 to ~710 eV.^{31–35} Other previously reported spectral features were also

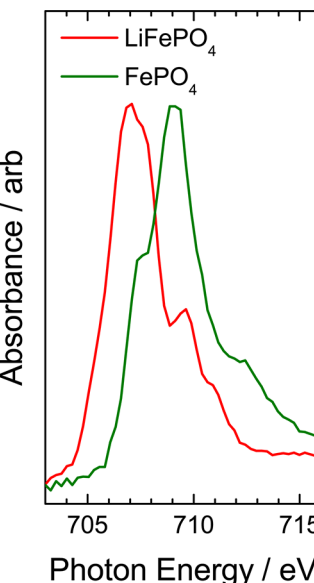


Figure 1. Fe L_3 X-ray absorption reference spectra taken from LiFePO₄ and FePO₄ electrodes lithiated and delithiated electrochemically.

satisfactorily reproduced. Spatially resolved state-of-charge (Fe³⁺ molar fraction) maps were obtained by least-squares fitting of STXM spectral images to a linear combination of the FePO₄ and LiFePO₄ reference spectra³⁶ using the Axis2000 software package.³⁷ For the electrode half-charged at 1 C, excellent fits were obtained at all spatial positions with a maximum residual of 0.8% (averaged over all photon energies). The LFP thickness at each pixel is obtained from the optical absorption using the appropriate material parameters. The average state-of-charge in each image is then the ratio of the average thicknesses of FePO₄ and LiFePO₄.

Three 5 × 5 μm regions centered at approximately 26, 18, and 6 μm from the Al current collector, respectively were analyzed. Figure 2 shows the SXTM maps, where the hue shows the state-of-charge with pure red representing 0% (i.e., LiFePO₄), yellow 50%, and green 100% (i.e., FePO₄), and the brightness gives the relative thickness of the particles. For the three regions analyzed, we obtained 49–51% average state-of-charge. Not only is the state-of-charge independent of position along the thickness of the battery electrode, it is also essentially identical to the average, electrochemically determined state-of-charge. The excellent agreement between the state-of-charge determined electrochemically and via STXM validates our quantification strategy. It also establishes that the great majority of the LFP particles are electrochemically active. Further support comes from the analysis of the electrochemically prepared reference samples. The nominally fully discharged reference sample gave 1.5% state-of-charge, and the fully charged sample gave 98.3% state-of-charge (Supporting Information Figure S3). Thus, essentially all of the LFP electrode was being charged and discharged during electrochemical cycling. We do note that the capacity of our batteries is less than the theoretical value of 170 mAh g⁻¹. We hypothesize that this deviation arises from: (1) non-LiFePO₄ material in the as-received electrode powder, and (2) nonuniformity in the electrode during preparation, leading to particles in specific parts of the electrode (such as its edges, which we do not image) becoming disconnected.

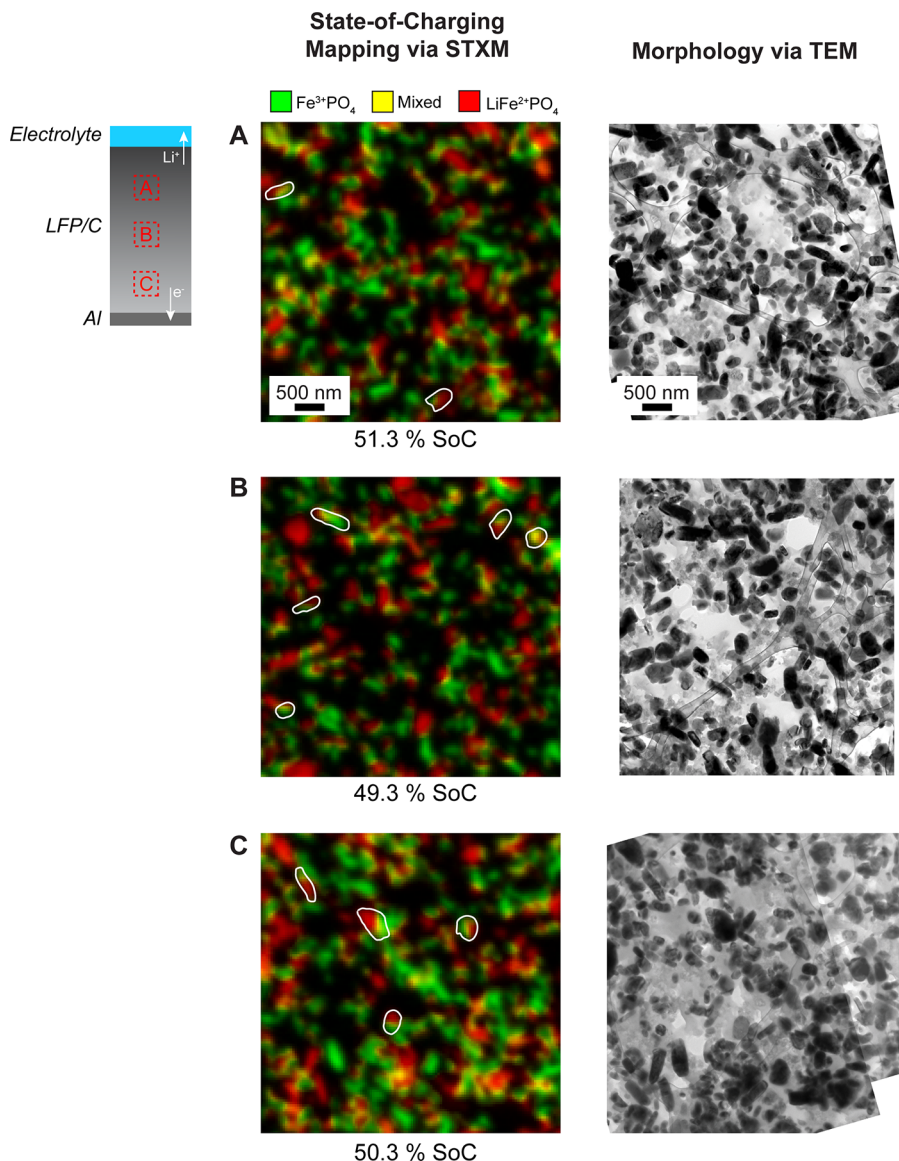


Figure 2. (Left) state-of-charge mapping obtained via scanning transmission X-ray microscopy and (right) morphology obtained via transmission electron microscopy of the same regions in the lithium iron phosphate composite electrode (A) 26 μm , (B) 18 μm (C) and 6 μm from the Al current collector. Hue and brightness give the local state-of-charge and lithium iron phosphate thickness, respectively. Outlined in white are particles in which two phases coexist within the same LFP particle; all other particles are single phase, either lithium-rich (red) or lithium-poor (green). Large netlike features in the TEM images are carbon grids in the sample holder.

A simple visual inspection of the STXM maps in Figure 2 reveals that there are significant inhomogeneities in the state-of-charge at the tens to hundreds of nanometer length scales, that is, adjacent particles have completely different states-of-charge. Notably, the extent of variation appears to be similar regardless of macroscopic position in the composite electrode, that is, close to the electrolyte (Figure 2A) or near the Al current collector (Figure 2C). Quantitative analysis provided in the Supporting Information (Figure S4) documents this long-range homogeneity. The absence of a gradient in lithium content on the electrode length scale indicates that the characteristic time of electron drift through the graphitic carbon and ion diffusion in the electrolyte is substantially faster than the charging time. In other words, there is no resistive loss to transport lithium from the surface of one particle to another.

Having established the absence of a macroscopic diffusion front within the LFP electrode, we now turn to the nanoscale

variation in the state-of-charge. We analyzed approximately 450 LFP individual particles. At first glance, many particles appear to exhibit state-of-charge ranging from 0 to 100%. However, because the two-dimensional STXM measurement averages through the thickness of the cross section, the charge state of overlapping particles are averaged in the maps. To resolve this ambiguity, we identified overlapping particles by imaging the same regions with TEM. The technique's high spatial resolution and large thickness contrast was used to identify the boundaries of the particles. No chemical information was obtained nor inferred from the TEM images. We first identify particle boundaries by superimposing the TEM images (Figure 2, right column) with the STXM state-of-charge maps (Figure 2, left column). State-of-charge data in regions where particles overlapped are not considered further. Next, we identified all particles containing multiple states-of-charge within each particle, that is, particles containing both red and green hues

in Figure 2. We labeled these particles as having a mixed state. The remaining particles mostly had a uniform state-of-charge of either above 95% or below 5% with the exception of particles edges which have values essentially above 85% or below 15% (see Supporting Information for details). The slight nonuniformities at the particles edges results from weak X-ray absorption, leading to larger errors on the spectral fitting. To reduce the impact of these artifacts, we label particles with state-of-charge above 85% as lithium-poor and below 15% as lithium-rich. Because of the STXM's spatial resolution, some well-isolated LFP particles present in TEM images were not analyzed. A total of 22 particles were omitted, compared to the 453 particles analyzed. Supporting Information Figure S6 gives the size distribution of particles based solely on the TEM image, and those based on a combination of TEM image and STXM mapping. These omissions are statistically insignificant.

Our analysis reveals that almost all scan locations that indicate an intermediate state-of-charge (yellow in Figure 2) are in fact overlapped particles. As summarized in Table 1, of the

Table 1. Statistics on the State-of-Charge of Lithium Iron Phosphate in a Composite Electrode, Sampled Either As a Cross Section or after Dispersing the Particles^a

	cross-sectioned electrode			dispersed electrode
	region A	region B	region C	total
number of particles	142	167	144	453
fraction of lithium-poor particles	68%	68%	60%	65%
fraction of lithium-rich particles	31%	29%	37%	32%
fraction of mixed particles	1.4%	3.0%	2.8%	2.4%
				3.7%

^aRegions in cross-sectioned electrode are indicated in Figure 2.

453 LFP particles examined, 65% are lithium-poor (green hue) meaning that they are nearly charged. On the other hand, 32% are lithium-rich (red hue), that is, they are nearly discharged. Only 11 particles (2%) exhibit intermediate states-of-charge (outlined in white in Figure 2). All of these particles contain phase boundaries separating lithium-rich and lithium-poor regions (resolution limitation of STXM prevents a meaningful analysis of the FePO₄/LiFePO₄ interface). Only these particles were actively charging when the charging was terminated. The time needed to charge these few particles is then ~50 times smaller than the time needed to charge the entire battery electrode. Even without further analysis, our results directly show that the transformation kinetics proceed rapidly once they are initiated within a particle, as suggested by previous experimental results.¹³

We also performed image analysis on the STXM maps and TEM images to correlate the state-of-charge to LFP particle dimensions. Since most particles are ellipsoidal, we carried out the size distribution analysis using the square root of the particle area and the longest and shortest line that goes through the particle's center of gravity (essentially the length of the long and short axes, respectively). All measures of particle size gave similar correlation between state-of-charge and size (Supporting Information Figures S7 and S8). For simplicity, we present the state-of-charge distribution as a function of the length of the long axis. The size distributions of lithium-rich and lithium-poor LFP particles (Figure 3A) show some differences. The average particle size (length of the long axis) is 256 nm for

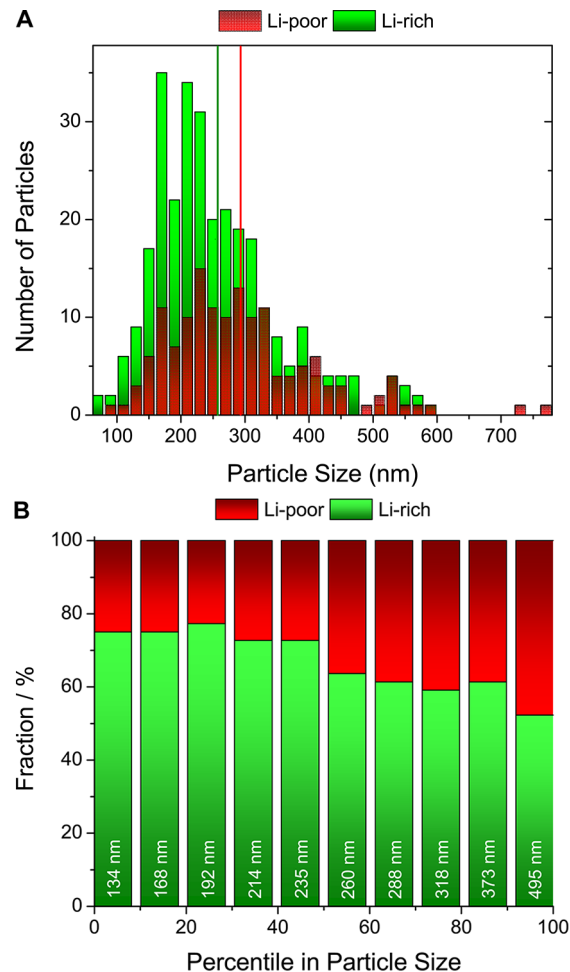


Figure 3. Particle-size distributions of all the single-phase particles shown in Figure 2. Vertical lines depict the average particle size. (A) Number of particles vs size. (B) The fraction of delithiated particles plotted as a function of percentile of particle size (in increments of 10%). Average particle size in each percentile range also shown. Each bar consists of 44 particles.

lithium-poor LFP and 294 nm for lithium-rich particles. In other words, lithium-rich particles are, on average, larger than the lithium-poor particles, and therefore store more charge per particle. The difference in the averaged particle size resolves the apparent discrepancy that 65% of the particles are lithium-poor for our half-charged electrode. At first, the difference in the average size seems to suggest that smaller particles are delithiated preferentially. However, a closer investigation of the size distribution of the two phases reveals that a substantial number of small and large particles still remain lithiated and delithiated, respectively. Figure 3B shows the fraction of lithium-rich and lithium-poor LFP particles as a function of the percentile in particle size (plotted in increments of 10%). For our half-charged electrode, 25% of the smallest particles (with an average size of 134 nm) remain lithiated. Similarly, 53% of the largest particles (with an average size of 495 nm) are delithiated. Thus, the probability of finding a particular LFP particle in either lithiation state depends only weakly on its size.

Since a macroscopic diffusion front was absent in our LFP electrode, we further improved the confidence of our analysis by imaging particles with reduced overlap prepared by dispersing the electrode. LFP powder scraped from the same electrode was suspended by sonication in anhydrous ethanol,

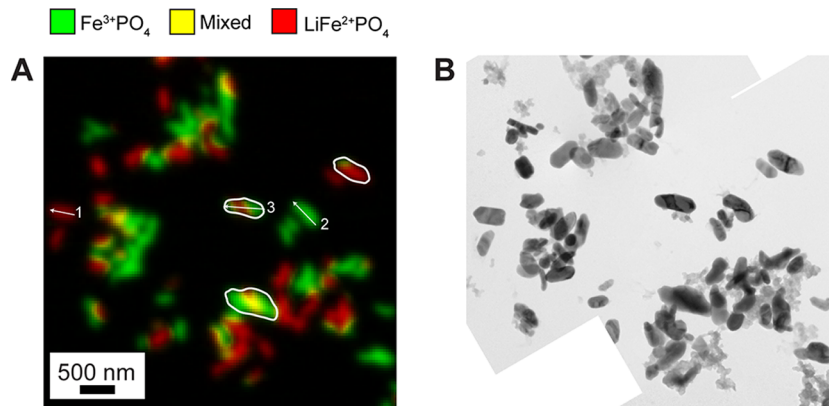


Figure 4. (A) State-of-charge mapping and (B) morphology of lithium iron phosphate electrode powder dispersed by sonication. From the same electrode shown in Figure 2. Outlined in white are particles in which two phases coexist within the same particle.

which was then pipetted onto a thin Si_3N_4 membrane. The STXM map and TEM image, Figure 4, show considerably better interparticle isolation than those of the cross-sectioned electrode. All of the experimental features discussed above were reproduced with the dispersed powder sample: (1) strong heterogeneity in the local state-of-charge, (2) 61% of the particles are lithium-rich and 36% are lithium-poor, and (3) only 3 out of the 81 particles are actively undergoing delithiation. X-ray absorption line scans across a lithium-poor, a lithium-rich, and a two-phase particle are shown in Figure 5.

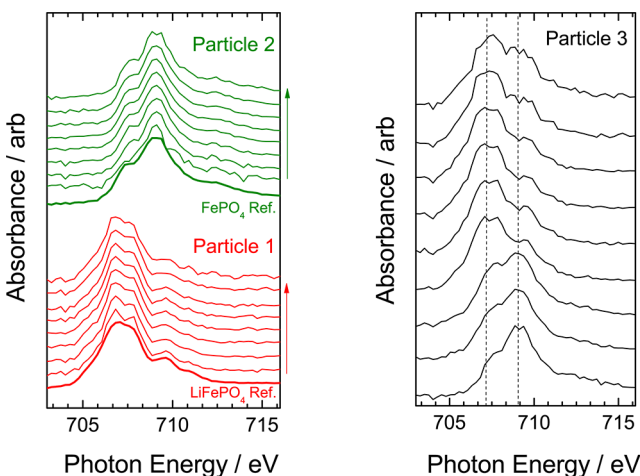


Figure 5. X-ray absorption line scans of select lithium iron phosphate particles indicated in Figure 4. Particles 1 and 2 are single phase and the X-ray absorption spectra showed negligible variations within the particle. Particle 3 contains two phases, separated by a well-defined boundary. Reference spectra (heavy lines) of the limiting compositions are also shown for comparison.

Summarizing our experimental results, we directly observed that lithium-rich and lithium-poor LFP particles dominated the electrode, and only ~2% of the particles were undergoing delithiation. These observations establish unambiguously that the particle-by-particle pathway is the prevailing many-particle intercalation route under the conditions examined. Furthermore, contrary to the common expectation that smaller particles would delithiate before larger ones, we observed only a weak correlation between the state-of-charge and the particle size. Next, we use these quantitative observations to elucidate the physical origin of the particle-by-particle pathway

and to give insights into the processes that limit delithiation in many-particle LFP electrodes.

When a stable phase boundary forms upon deintercalation, its lithium chemical potential is at a value higher than that of the electrolyte. This overpotential constitutes the driving force of the phase transformation, that is, for moving the phase boundary. While forming the phase boundary perturbs the lithium chemical potential of the electrolyte and single-phase particles,^{6,28} the perturbation is vanishingly small for a real battery electrode with fast interparticle transport, such as ours. That is, the electrolyte and/or particles in the electrode act as reservoirs that can rapidly sink (or source) lithium. We next consider two phenomena that can plausibly limit the rate of phase transformation in LFP: (1) the initiation of phase transformation (e.g., a nucleation-like event), and (2) the propagation of the phase boundary (i.e., the growth of a lithium-poor phase within the particle during deintercalation).

If the energetic barrier of a nucleation-like event is large compared to that of boundary propagation, the supersaturation needed to achieve the required nucleation rate sets the electrode overpotential. This overpotential also readily propagates the phase boundary. At a given overpotential, the time needed to complete a particle's transformation is small compared to the average time needed to initiate nucleation. Thus, we expect the number of particles undergoing transformation to be much smaller than the total number of particles, which is precisely what we observe in the LFP electrode. In this limit the charging current is equal to the nucleation rate times the average particle charge, and the overpotential required to attain a particular charging rate is determined by the nucleation rate, not by the phase-boundary velocity.

Our observations are inconsistent with the other limiting regime, where propagation of the phase boundary (controlled by, for example, lithium diffusion or surface reaction) sets the overpotential. In this limit, the overpotential that gives significant nucleation rates is insufficient to sweep a boundary through a particle before nucleation events occur in other particles. Then, most particles should transform at the same time, unless the boundary motion has a strong dependence on size. But we have found no such dependence (see Figure 3). Our statistics with ~2% particles transforming at once show that our LFP electrode is far from being in this regime.

Additionally, our observations also suggest that charging in LFP could not have proceeded via the recently proposed solid-

solution pathway, where no phase separation occurs throughout charging. Similar to the two-phase transformation pathway limited by boundary propagation, LFP particles undergoing a solid-solution pathway would start charging concurrently. For a half-charged electrode with no electrolyte transport limitations, we would expect to see a significant fraction of the particles in an intermediate state-of-charge. This was not observed, at least for a 1 C charging rate.

Having established that charging in LFP is limited by the initiation of phase transformation, we now turn to the particle size distribution of the lithium-rich and lithium-poor phases. The size distributions of particles that have yet to transform and those that have already transformed give us insights into the probability of initiating phase transformation as a function of particle size. In the nucleation-limited regime, we expect that the nucleation probability to correlate monotonically with the surface area of the particles (for heterogeneous nucleation), provided that the barrier height is independent of particle size and morphology. However, this was not observed in our experiment (Figure 3b). Our results likely indicate a nontrivial (and possibly nonmonotonic) dependence of nucleation barrier height on the particle size (and maybe also on morphology). One possibility is that the extent and nature of carbon-coating depends on particle size and morphology,^{38,39} which subsequently leads to significant variations between particles. Detailed correlation of particle surface characteristics and the sequence of transformation is underway.

In summary, we have combined the high chemical and spatial resolutions of STXM and TEM, respectively, to map the state-of-charge in individual LFP particles over the entire thickness of a battery electrode. The average lithium content of the particles did not vary with distance from the current collector, establishing that Li transport through the electrolyte is relatively fast under a 1 C charging current. When the entire electrode was charged to 50%, almost all the LFP particles are nearly completely charged or discharged. This is the mosaic limit of a transforming particle ensemble. Furthermore, only a small fraction of the particles (~2%), those with both lithium-rich and lithium-poor regions, are undergoing phase transformation at one time. Therefore, the time needed to charge individual LFP particles completely is much shorter (about 50 times) than the time needed to charge the entire particle ensemble. These observations establish that the rate of initiating the phase transformation in a particle is much slower than the rate of completing the phase transformation. Furthermore, the sequence of delithiation depends only weakly on the particle size, and, subsequently, on the particle's surface area. This finding suggests that the barrier height for nucleation-like events scale with particle size in a nonlinear and possibly nonmonotonic manner. This work provides direct guidance for how to improve the performance of LFP battery electrodes, namely, by increasing the rate of the nucleation-like events.

■ ASSOCIATED CONTENT

Supporting Information

Materials and methods, and battery electrochemical characterizations, particle size distribution, and state-of-charge analysis. This material is available free of charge via the Internet at <http://pubs.acs.org>.

■ AUTHOR INFORMATION

Corresponding Author

*Email: wchueh@stanford.edu.

Present Address

[†]Department of Materials Science and Engineering, Stanford University, California 94305, United States.

Notes

The authors declare no competing financial interest.

■ ACKNOWLEDGMENTS

The research was supported by the U.S. Department of Energy through the Sandia Laboratory Directed research and Development program under Contract DE-AC04-94AL85000. The Advanced Light Source is supported by the Director, Office of Science, Office of Basic Energy Sciences, of the U.S. Department of Energy under Contract No. DE-AC02-05CH11231. W.C.C. was also supported by an appointment to the Sandia Truman Fellowship in the National Security Science and Engineering. F.E.G., K.R.Z., N.C.B., and K.F.M. acknowledge support from the Office of Basic Energy Science, Division of Materials Sciences and Engineering. W.L. acknowledges Michigan State University for providing the start-up package. Finally, the authors are grateful to A.L.D. Kilcoyne at the Advanced Light Source for his assistance with the X-ray microscopy experiments, M. Homer at Sandia for preparing samples, and Y. Li at Stanford for data analysis.

■ REFERENCES

- (1) Padhi, A. K.; Nanjundaswamy, K. S.; Goodenough, J. B. Phospho-olivines as positive-electrode materials for rechargeable lithium batteries. *J. Electrochem. Soc.* **1997**, *144*, 1188–1194.
- (2) Han, B. C.; Ven, A. V. d.; Morgan, D.; Ceder, G. Electrochemical modeling of intercalation processes with phase field models. *Electrochim. Acta* **2004**, *49*, 4691–4699.
- (3) Singh, G. K.; Ceder, G.; Bazant, M. Z. Intercalation dynamics in rechargeable battery materials: General theory and phase-transformation waves in LiFePO₄. *Electrochim. Acta* **2008**, *53*, 7599–7613.
- (4) Burch, D.; Bazant, M. Z. Size-Dependent Spinodal and Miscibility Gaps for Intercalation in Nanoparticles. *Nano Lett.* **2009**, *9*, 3795–3800.
- (5) Van der Ven, A.; Garikipati, K.; Kim, S.; Wagemaker, M. The Role of Coherency Strains on Phase Stability in Li_xFePO₄: Needle Crystallites Minimize Coherency Strain and Overpotential. *J. Electrochem. Soc.* **2009**, *11*, A949–A957.
- (6) Dreyer, W.; et al. The thermodynamic origin of hysteresis in insertion batteries. *Nat. Mater.* **2010**, *9*, 448–453.
- (7) Lai, W. Electrochemical modeling of single particle intercalation battery materials with different thermodynamics. *J. Power Sources* **2010**, *196*, 6534–6553.
- (8) Safari, M.; Delacourt, C. Mathematical Modeling of Lithium Iron Phosphate Electrode: Galvanostatic Charge/Discharge and Path Dependence. *J. Electrochem. Soc.* **2011**, *158*, A63–A73.
- (9) Ramana, C. V.; Mauger, A.; Gendron, F.; Julien, C. M.; Zaghib, K. Study of the Li-insertion/extraction process in LiFePO₄/FePO₄. *J. Power Sources* **2009**, *187*, 555–564.
- (10) Malik, R.; Zhou, F.; Ceder, G. Kinetics of non-equilibrium lithium incorporation in LiFePO₄. *Nat. Mater.* **2011**, *10*, 587–590.
- (11) Bai, P.; Cogswell, D. A.; Bazant, M. Z. Suppression of Phase Separation in LiFePO₄ Nanoparticles During Battery Discharge. *Nano Lett.* **2011**, *11*, 4890–4896.
- (12) Cogswell, D. A.; Bazant, M. Z. Coherency Strain and the Kinetics of Phase Separation in LiFePO₄ Nanoparticles. *ACS Nano* **2012**, *6*, 2215–2225.

- (13) Delmas, C.; Maccario, M.; Croguennec, L.; Cras, F. L.; Weill, F. Lithium deintercalation in LiFePO_4 nanoparticles via a domino-cascade model. *Nat. Mater.* **2008**, *7*, 665–671.
- (14) Meethong, N.; et al. Electrochemically Induced Phase Transformation in Nanoscale Olivines $\text{Li}_{1-x}\text{MPO}_4$ (M) Fe, Mn). *Chem. Mater.* **2008**, *20*, 6189–6198.
- (15) Kao, Y.-H.; et al. Overpotential-Dependent Phase Transformation Pathways in Lithium Iron Phosphate Battery Electrodes. *Chem. Mater.* **2010**, *22*, 5845–5855.
- (16) Badi, S.-P.; et al. Direct synthesis of nanocrystalline $\text{Li}_{0.90}\text{FePO}_4$: observation of phase segregation of anti-site defects on delithiation. *J. Mater. Chem.* **2011**, *21*, 10085–10093.
- (17) Sharma, N.; et al. Direct Evidence of Concurrent Solid-Solution and Two-Phase Reactions and the Nonequilibrium Structural Evolution of LiFePO_4 . *J. Am. Chem. Soc.* **2012**, *134*, 7867–7873.
- (18) Gibot, P.; et al. Room-temperature single-phase Li insertion/extraction in nanoscale Li_xFePO_4 . *Nat. Mater.* **2008**, *7*, 741–747.
- (19) Laffont, L.; et al. Study of the $\text{LiFePO}_4/\text{FePO}_4$ Two-Phase System by High-Resolution Electron Energy Loss Spectroscopy. *Chem. Mater.* **2006**, *5520–5529*.
- (20) Chen, G.; Song, X.; Richardson, T. J. Electron Microscopy Study of the LiFePO_4 to FePO_4 Phase Transition. *Electrochim. Solid State* **2006**, *9*, A295–A298.
- (21) Brunetti, G.; et al. Confirmation of the Domino-Cascade Model by $\text{LiFePO}_4/\text{FePO}_4$ Precession Electron Diffraction. *Chem. Mater.* **2011**, *23*, 4515–4524.
- (22) Gu, L.; et al. Direct Observation of Lithium Staging in Partially Delithiated LiFePO_4 at Atomic Resolution. *J. Am. Chem. Soc.* **2011**, *133*, 4661–4663.
- (23) Allen, J. L.; Low, T. R.; Wolfenstine, J. Kinetic Study of the Electrochemical FePO_4 to LiFePO_4 Phase Transition. *Chem. Mater.* **2007**, *19*, 2108–2111.
- (24) Oyama, G.; Yamada, Y.; Natsui, Y.; Nishimura, S.; Yamada, A. Kinetics of Nucleation and Growth in Two-Phase Electrochemical Reaction of Li_xFePO_4 . *J. Phys. Chem. C* **2012**, *116*, 7306–7311.
- (25) Liu, J.; Kunz, M.; Chen, K.; Tamura, N.; Richardson, T. J. Visualization of Charge Distribution in a Lithium Battery Electrode. *J. Phys. Chem. Lett.* **2010**, *1*, 2120–2123.
- (26) Wagemaker, M.; Borghols, W. J. H.; Mulder, F. M. Large impact of particle size on insertion reaction. A case for anatase Li_xTiO_2 . *J. Am. Chem. Soc.* **2007**, *129*, 4323–4327.
- (27) Wagemaker, M.; Mulder, F. M.; Van der Ven, A. The Role of Surface and Interface Energy on Phase Stability of Nanosized Insertion Compounds. *Adv. Mater.* **2009**, *21*, 2703–2709.
- (28) Burch, D. *Intercalation Dynamics in Li-ion Batteries*; Ph.D thesis, Massachusetts Institute of Technology, Cambridge, Massachusetts, 2009.
- (29) Kilcoyne, A. L. D.; et al. Interferometer-controlled scanning transmission X-ray microscopes at the Advanced Light Source. *J. Synchrotron Radiat.* **2003**, *10*, 125–136.
- (30) Lee, K. T.; Kan, W. H.; Nazar, L. F. Proof of Intercrystallite Ionic Transport in LiMPO_4 Electrodes (M) Fe, Mn). *J. Am. Chem. Soc.* **2009**, *131*, 6044–6045.
- (31) Augustsson, A.; et al. Electronic structure of phospho-olivines Li_xFePO_4 ($x = 0, 1$) from soft-x-ray-absorption and -emission spectroscopies. *J. Chem. Phys.* **2005**, *123*, 184717.
- (32) Hunt, A.; Ching, W.-Y.; Chiang, Y.-M.; Moewes, A. Electronic structures of LiFePO_4 and FePO_4 studied using resonant inelastic x-ray scattering. *Phys. Rev. B* **2006**, *73*, 205120.
- (33) Kurosumi, S.; et al. Resonant Photoemission Spectroscopy of the Cathode Material Li_xFePO_4 for Lithium Ion Battery. *J. Phys. Chem. C* **2011**, *115*, 25519–25522.
- (34) Wang, X.-J.; et al. Investigation of the structural changes in $\text{Li}_{1-x}\text{FePO}_4$ upon charging by synchrotron radiation techniques. *J. Mater. Chem.* **2011**, *21*, 11406–11411.
- (35) Yang, S.; et al. Soft X-ray XANES studies of various phases related to LiFePO_4 based cathode materials. *Energy Environ. Sci.* **2012**, *5*, 7007–7016.
- (36) Liu, X.; et al. Phase Transformation and Lithiation Effect on Electronic Structure of Li_xFePO_4 : An In-Depth Study by Soft X-ray and Simulations. *J. Am. Chem. Soc.* **2012**, In Press.
- (37) Setoguchi, T.; Okamoto, K.; Eguchi, K.; Arai, H. Effects of anode material and fuel on anodic reaction of solid oxide fuel cells. *J. Electrochem. Soc.* **1992**, *139*, 2875–2880.
- (38) Chen, Z.; Dahn, J. R. Reducing Carbon in LiFePO_4 OC Composite Electrodes to Maximize Specific Energy, Volumetric Energy, and Tap Density. *J. Electrochem. Soc.* **2002**, *149*, A1184–A1189.
- (39) Trudeau, M. L.; et al. In situ high-resolution transmission electron microscopy synthesis observation of nanostructured carbon coated LiFePO_4 . *J. Power Sources* **2011**, *196*, 7383–7394.